Technical Report

486

W. D. Fitzgerald

Limited Electronic Scanning with an Offset-Feed Near-Field Gregorian System

24 September 1971

Prepared for the Office of the Chief of Research and Development,
Department of the Army,
under Electronic Systems Division Contract F19628-70-C-0230 by

Lincoln Laboratory

MASSACHUSETTS INSTITUTE OF TECHNOLOGY

Lexington, Massachusetts

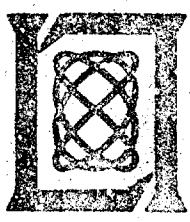

DOCUMENT CONTROL DATA - R&D

(Security classification of title, body of abstract and indexing annotation must be entered when the overall report is classified)

1. ORIGINATING ACTIVITY (Corporate author) Lincoln Laboratory, M.I.T.	2a. REPORT SECURITY CLASSIFICATION Unclassified 2b. GROUP None

3. REPORT TITLE

Limited Electronic Scanning with an Offset-Feed Near-Field Gregorian System

4. DESCRIPTIVE NOTES (Type of report and inclusive dates)
Technical Report

5. AUTHOR(S) (Last name, first name, initial)

Fitzgerald, William D.

6. REPORT DATE	7a. TOTAL NO. OF PAGES	7b. NO. OF REFS
24 September 1971	32	4

8a. CONTRACT OR GRANT NO. F19628-70-C-0230 b. PROJECT NO. 7X263304D215 c. d.	9a. ORIGINATOR'S REPORT NUMBER(S) Technical Report 486 9b. OTHER REPORT NO(S) (Any other numbers that may be assigned this report) ESD-TR-71-272

10. AVAILABILITY/LIMITATION NOTICES

Approved for public release; distribution unlimited.

11. SUPPLEMENTARY NOTES	12. SPONSORING MILITARY ACTIVITY
None	Office of the Chief of Research and Development, Department of the Army

13. ABSTRACT

The scanning characteristics of an offset-feed near-field Gregorian antenna excited with a planar array are investigated. The analysis is based on the assumption that the fields in the near-zone region of the array can be accurately determined by the methods of ray optics, i.e., geometrical propagation along ray trajectories. Scalar diffraction theory is used to compute secondary characteristics. For one example considered, a 1/2° beam is scanned over a cone with a half angle of approximately 7° as defined by the −3-dB scan-loss criterion. The effects of changing parameters – magnification, reflector sizes, frequency, etc. – on the scan characteristics are discussed. An experiment which was performed to demonstrate the technique is described.

14. KEY WORDS

electronic scanning
Gregorian antenna
planar array
beam-forming networks
reflectors
off-axis feed
ray optics

ABSTRACT

The scanning characteristics of an offset-feed near-field Gregorian antenna excited with a planar array are investigated. The analysis is based on the assumption that the fields in the near-zone region of the array can be accurately determined by the methods of ray optics, i.e., geometrical propagation along ray trajectories. Scalar diffraction theory is used to compute secondary characteristics. For one example considered, a 1/2° beam is scanned over a cone with a half angle of approximately 7° as defined by the −3-dB scan-loss criterion. The effects of changing parameters — magnification, reflector sizes, frequency, etc. — on the scan characteristics are discussed. An experiment which was performed to demonstrate the technique is described.

Accepted for the Air Force
Joseph R. Waterman, Lt. Col., USAF
Chief, Lincoln Laboratory Project Office

MASSACHUSETTS INSTITUTE OF TECHNOLOGY
LINCOLN LABORATORY

LIMITED ELECTRONIC SCANNING WITH AN OFFSET-FEED NEAR-FIELD GREGORIAN SYSTEM

W. D. FITZGERALD

Group 34

TECHNICAL REPORT 486

24 SEPTEMBER 1971

LEXINGTON MASSACHUSETTS

The work reported in this document was performed at Lincoln Laboratory, a center for research operated by Massachusetts Institute of Technology. The work is sponsored by the Office of the Chief of Research and Development, Department of the Army; it is supported by the Advanced Ballistic Missile Defense Agency under Air Force Contract F19628-70-C-0230.

CONTENTS

LIMITED ELECTRONIC SCANNING WITH AN OFFSET-FEED NEAR-FIELD GREGORIAN SYSTEM

I. INTRODUCTION

Limited-scan-antenna techniques, which combine mechanical and some degree of electronic beam steering have application in systems which must acquire and track a number of targets within a limited angular region centered on the mechanical axis. Recently, the near-field Cassegrainian antenna which utilizes confocal paraboloids and a relatively small planar-array feed was shown to have some attractive features as a limited-scan system.[1] Over the limited range of scan afforded, the system combines the high resolution and (to a large degree) the low cost of a reflector antenna with the performance capabilities of an electronically scanned array.

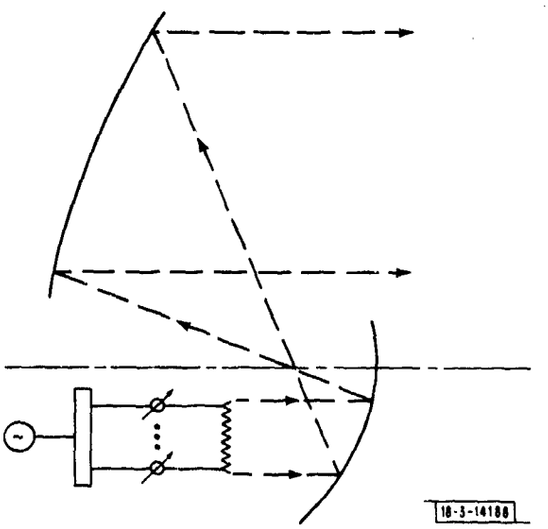

Fig. 1. Offset-feed Gregorian geometry.

To achieve good scan range with the near-field Cassegrainian system, the subreflector and consequently the blockage ratio must be relatively large. The resulting degradation of the efficiency and sidelobe characteristics is the main disadvantage of this technique. A variation on the basic theme, which we will investigate here, is the offset-feed near-field Gregorian geometry shown schematically in Fig. 1. The subreflector is well into the near-field of the array and both reflectors are offset sections of confocal, coaxial paraboloids. Dudkovsky[2] proposed this configuration for efficiently illuminating a large reflector, and Skahill, et al.[3] first investigated the off-axis properties of the system.

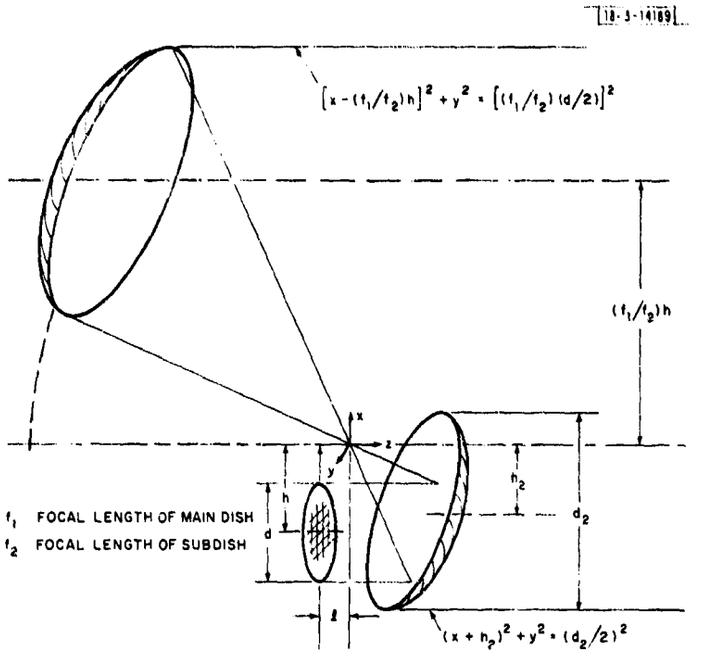

Fig. 2. Parameters defining offset-feed configuration.

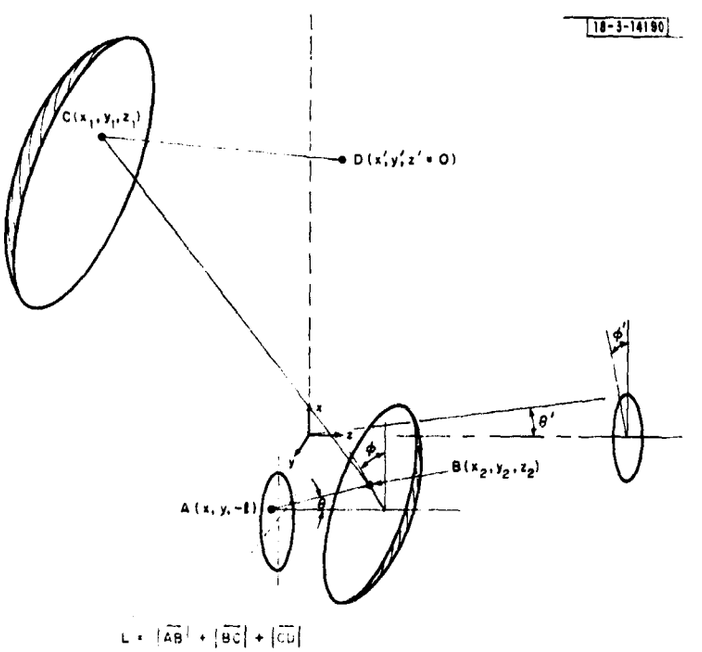

Fig. 3. Path of general ray showing coordinates θ, φ and θ', φ'.

The advantages of the offset-feed geometry as opposed to the circularly symmetric Cassegrainian are:

(a) Blockage is eliminated; the efficiency and sidelobes are not sacrificed when using the larger subreflectors required for increased scan coverage.

(b) Spillover, the main cause of scan loss with the Cassegrainian feed, is markedly reduced because the array can be positioned very close to an enlarged subreflector.

Both systems enjoy the absence of "coma" commonly associated with the off-axis properties of a paraboloid. The offset-feed geometry is applicable to circular sections of paraboloids as well as to parabolic cylinders. The latter configuration would result in a prohibitive amount of blocking with the Cassegrainian approach.

Interest in this technique was generated by the desire for an electronically scanned array for the measurements program at the Western Test Range. Field experiments on a multiple-target complex made at long ranges, e.g., pertaining to area or regional defense concepts, would require an array with high sensitivity and high resolution, but a limited field of view would suffice. At shorter ranges, measurements associated with the Hardsite defense concept would require an array with much greater scan coverage but with reduced sensitivity requirements. An attractive feature of the offset-feed geometry is the possibility of satisfying both of these conflicting requirements by rapidly removing the subreflector to expose the array for use in the latter mode of operation. In simple terms, the array is fitted with a rapidly removable telescope for long-range viewing and, as with any telescope, the field of view is diminished in proportion to the magnification.

Our purpose is to evaluate the scanning capabilities of the three-dimensional near-field Gregorian geometry, i.e., circular sections of paraboloids, with an analysis based on ray-tracing techniques and scalar diffraction theory. The analysis is based on the assumption that the fields in the near-zone region of the array (the distance to the subreflector) are accurately determined by the methods of ray otpics. We will also describe an experiment which was performed to verify the technique.

II. ANALYSIS

Figure 2 shows the parameters which define the geometry. Both reflectors shown are sections of confocal paraboloids which are circular when projected into the x-y plane. The main reflector is that portion of the complete paraboloid intersected by the cylinder $[x - (f_1/f_2)\, h]^2 + y^2 = [(f_1/f_2)\,(d/2)]^2$; similarly, the subreflector outline is defined by the cylinder $(x + h_2)^2 + y^2 = (d_2/2)^2$. The main aperture when defined in this manner is completely utilized for the boresight beam. Just as with the near-field Cassegrainian system, there is no space attenuation with the offset-feed geometry. The form of the amplitude distribution applied to the array is reproduced over the main aperture without alteration.

The subreflector is illuminated with a linear phase front by placing it well into the near-field of the array. The secondary beam is scanned simply by generating a linear phase tilt on the array. If Θ, φ are the coordinates which define the phase tilt of the array, and Θ', φ' are the spherical coordinates defining the secondary-beam position (see Fig. 3), then for small angles,

$$\Theta = (f_1/f_2)\,\Theta'$$

$$\varphi = \varphi' + \pi \quad . \tag{1}$$

Unfortunately, Eq. (1) applies only for a few beamwidths scan from boresight. Over most of the interesting scan range, the relationship between the two sets of coordinates is nonlinear.

The objective of the ray-tracing procedure is to determine the amplitude and phase distribution over the main aperture plane as a function of the known amplitude and linear phase distributions on the array aperture. Scalar diffraction theory is then used to evaluate the secondary characteristics of the system. It should be noted that diffraction effects arising from the near-field assumption and the edge effects associated with both reflectors are not part of the analysis.

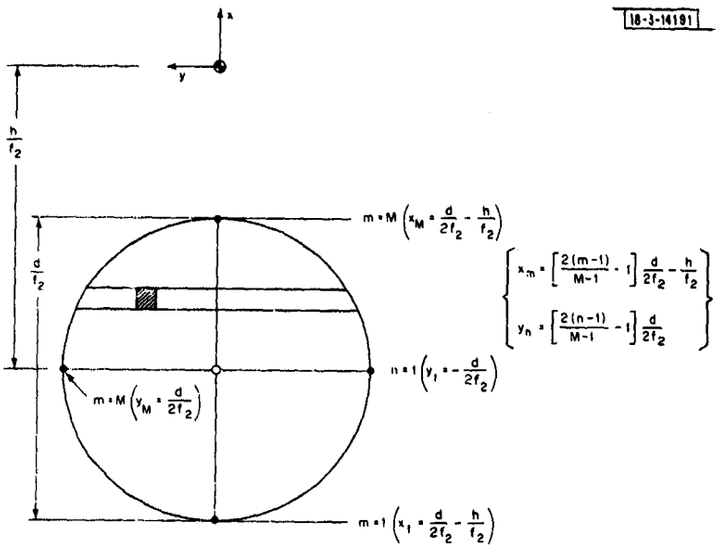

Fig. 4. Subdivision of array aperture for numerical analysis.

Figure 4 illustrates how the array aperture is divided into a two-dimensional lattice of equally spaced sampling points. The index M sets the number of rays traced as well as the number of sampling points on the main aperture. This parameter determines the trade-off between computational labor and the accuracy of the computed patterns. For each pair of coordinate points x_m, y_n and for a given θ, φ, the coordinates of the points of reflection which describe the passage of the ray through the system are computed and then used to determine the optical path length $L_{m,n}$. The parameters d, h, ℓ, h_2, d_2 and the coordinates of points on the array and subreflector are normalized to f_2. The coordinates of the main reflector and the assumed aperture plane are normalized to f_1. The phase distribution over the main aperture is given by

$$\Phi(x'_{m,n}; y'_{m,n}) = 2\pi(f_2/\lambda)\left\{\sin\theta\left[\left(x_m + \frac{h}{f_2}\right)\cos\varphi + y_n \sin\varphi\right] + (f_1/f_2)\,(L_{m,n}/f_1)\right\} \quad . \qquad (2)$$

This phase function is simply the sum of the linear phase shift applied to the array and the electrical path length as determined by ray tracing.

The amplitude distribution over the main aperture plane, denoted $E'(x'_{m,n}; y'_{m,n})$, is related to the assumed distribution on the array by conservation of energy in ray optics. Thus,

$$\Delta x \Delta y E^2(x_m, y_n) = (f_1/f_2)^2\, \Delta x'_{m,n} \Delta y'_{m,n} E'^2(x'_{m,n}; y'_{m,n}) \qquad (3)$$

or

$$E'(x'_{m,n}; y'_{m,n}) = (f_2/f_1)\ \frac{2}{M-1}\ (d/2f_2)\ \frac{E(x_m, y_n)}{\sqrt{\Delta x'_{m,n}\Delta y'_{m,n}}}$$

where

$$\Delta x = \Delta y = \frac{2}{M-1}\ (d/2f_2)$$

$$\Delta x'_{m,n} = x'_{m+1,n} - x'_{m,n}$$

$$\Delta y'_{m,n} = y'_{m,n+1} - y'_{m,n} \quad .$$

The pattern $P(\theta', \varphi')$ is computed with the well-known expression from scalar diffraction theory in summation form:

$$P(\theta', \varphi') = \sum_m \sum_n \Delta x'_{m,n}\Delta y'_{m,n} E'(x'_{m,n}; y'_{m,n}) \exp[-j\Phi(x'_{m,n}; y'_{m,n})]$$
$$\times \exp[j2\pi(f_1/f_2)\ (f_2/\lambda)\ \sin\theta'(x'_{m,n}\cos\varphi' + y'_{m,n}\sin\varphi')] \quad . \tag{4}$$

By combining Eqs. (3) and (4) and omitting unnecessary constants,

$$|P(\theta', \varphi')| = \left| \sum_{m=1}^{M} \sum_{n=1}^{M} \sqrt{\Delta x'_{m,n}\Delta y'_{m,n}} E(x_m, y_n) \exp[-j\Phi(x'_{m,n}; y'_{m,n})] \right.$$
$$\left. \times \exp[j2\pi(f_1/f_2)\ (f_2/\lambda)\ \sin\theta'(x'_{m,n}\cos\varphi' + y'_{m,n}\sin\varphi')] \right| \tag{5}$$

where $\Phi(x'_{m,n}; y'_{m,n})$ is given by Eq. (2). Rays which are spilled over either the subreflector or the main reflector are excluded in the ray-tracing portion of the program. The coordinates of a point of reflection on the subreflector $x_{2m,n}; y_{2m,n}$ must satisfy the inequality

$$[x_{2m,n} + (h_2/f_2)]^2 + y^2_{2m,n} \leqslant (d_2/2f_2)^2 \quad . \tag{6}$$

Similarly, a point $x_{1m,n}; y_{1m,n}$ on the main reflector must satisfy the inequality

$$[x_{1m,n} - (h/f_2)]^2 + y^2_{1m,n} \leqslant (d/2f_2)^2 \quad . \tag{7}$$

Table I lists the input parameters to the computer program. Following are some comments on the nature and restrictions of each of these parameters.

The index M determines the number of sampling points over the main aperture. In order to deal with a manageable computational load, we must restrict the pattern computations to the principal lobe and the first few near-in sidelobes. It is difficult to determine precisely the magnitude of M required. Methods available for numerical evaluation of diffraction integrals such as Newton-Coates, Gaussian quadrature, etc.,[4] are not directly applicable to our problem. A numerical investigation has shown that a value of M = 30 results in an error of less than 1.0 dB over the first three sidelobes. A value of M = 15 (approximately one-fourth the computational labor) accurately predicts scan loss and the form of the main beam, and was generally used when investigating the effect of varying parameters. A few of the more interesting configurations were then computed with M = 30.

TABLE I INPUT PARAMETERS TO THE COMPUTER PROGRAM	
M	Typically, $15 \leq M \leq 30$
θ φ	Array phase tilt
f_1/f_2	Magnification
h/f_2 d/f_2 ℓ/f_2 h_2/f_2 d_2/f_2	Geometrical parameters
f_2/λ	Frequency term
K C	Distribution on array

The coordinates θ, φ define the normal to the linear phase front assumed for the array and are not, in general, linearly related to the coordinates θ', φ' which define the position of the secondary beam. The program is designed to locate the secondary-beam peak with a maximizing routine before computing pattern cuts.

The linear magnification for the boresight beam ($\theta = 0$) is f_1/f_2. The increase in gain of the system relative to the gain of the array is a function of the magnification only and is given by

$$\frac{G_o}{G_{array}} = 10 \log (f_1/f_2)^2 \quad . \tag{8}$$

The geometrical parameters determine the size and positioning of the array as well as the two reflectors. The constraint (7), which defines the outline of the main reflector, can be modified or removed to investigate the effects of an "oversized" main reflector. When (7) is used, the main reflector is completely utilized for the boresight beam.

The parameters K and C determine the form of the amplitude distribution applied to the array. The expression used is

$$E(x_m, y_n) = \left\{ 1 - \frac{\left[\left(x_m + \frac{h}{f_2}\right)^2 + y_n^2\right]}{(d/2f_2)^2} \right\}^K + C \quad . \tag{9}$$

Hence K = 0, C = 0 corresponds to a uniform distribution; K = 1, C = 0 is a $(1 - \rho^2)$ distribution; etc. A full-wave sine difference distribution was also used in some cases to investigate the scanning characteristics of a typical error pattern.

III. COMPUTED RESULTS

The large number of parameters and the asymmetrical nature of the system preclude a simple set of curves to describe performance characteristics. We will consider an example in some detail and then discuss the influence of various parameters.

Figure 5 shows a cross section of the example considered. The magnification is 3.0 and the main reflector size (136λ) corresponds to a nominal 1/2° beam. An orthographic projection of

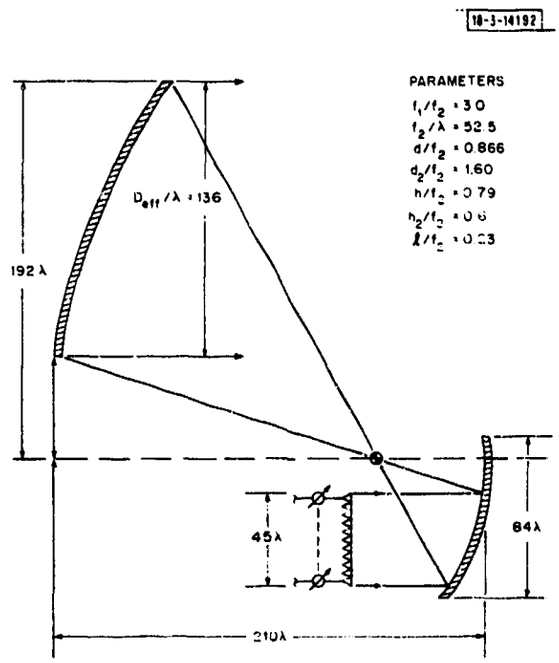

Fig. 5. Parameters of example with magnification of 3.0 and nominal 1/2° beam.

the far-field coordinates Θ', φ' is shown in Fig. 6. The −3-dB scan-loss contours are as indicated, and the circles represent (approximately) the −3-dB contour of the 1/2° beam. Note that the linear relationship between coordinate pairs [Eq. (1)] applies only for scanning a few beamwidths from boresight. Over most of the usable scan range, the relationship is nonlinear. For any plane φ = constant, the patterns are computed for 4° increments in Θ.

For the boresight beam, a real image (i.e., an airy disk) is created at the focal point of the reflectors. All power transmitted by the array is contained within an area on the order of a wavelength in diameter. As the array is scanned in the plane $\varphi = \pi$, this high-energy concentration, although somewhat diffused, approaches the top edge of the array. Hence, if Θ is allowed to exceed a certain value, a condition of near-total blockage can quickly result. The upper bound on Θ depends on the magnification and the position of the array. Typical limiting values are 16° to 18°. The cross-hatched region at the top of Fig. 6 indicates the approximate region where blockage can occur. The scan coverage with the $(1 - \rho^2)$ taper as defined by the −3-dB scan-loss criterion is a cone with a half angle of approximately 7° or 14 beamwidths.

Figures 7, 8 and 9 show the computed patterns for the $(1 - \rho^2)$ distribution in the three principal planes. In the vertical plane (Fig. 7), $\varphi = 0$, $\varphi' = \pi$ corresponds to scanning the array up and the secondary beam down. In this plane, the half-power beamwidths are constant, even beyond the −3-dB scan-loss point, but there is clear evidence of phase distortion. The implication

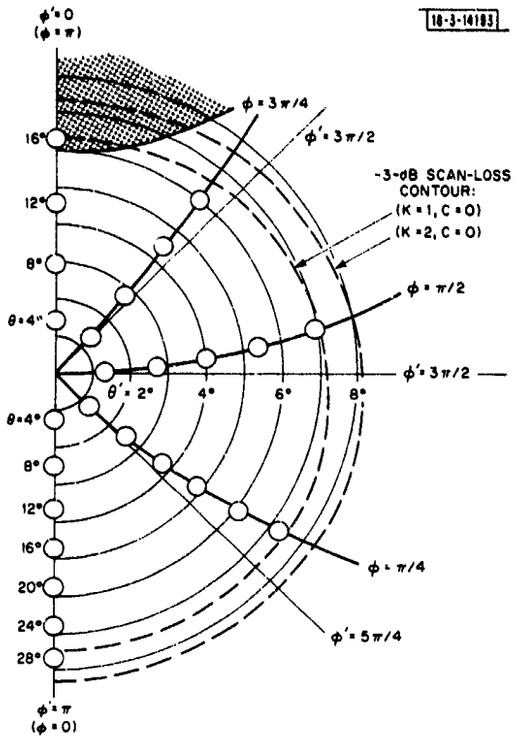

Fig. 6. Orthographic projection of coordinates θ', φ' showing nonlinear relationship between coordinate systems and scan-coverage contours. Circles represent 1/2° beams, and approximate region where blockage occurs is cross-hatched.

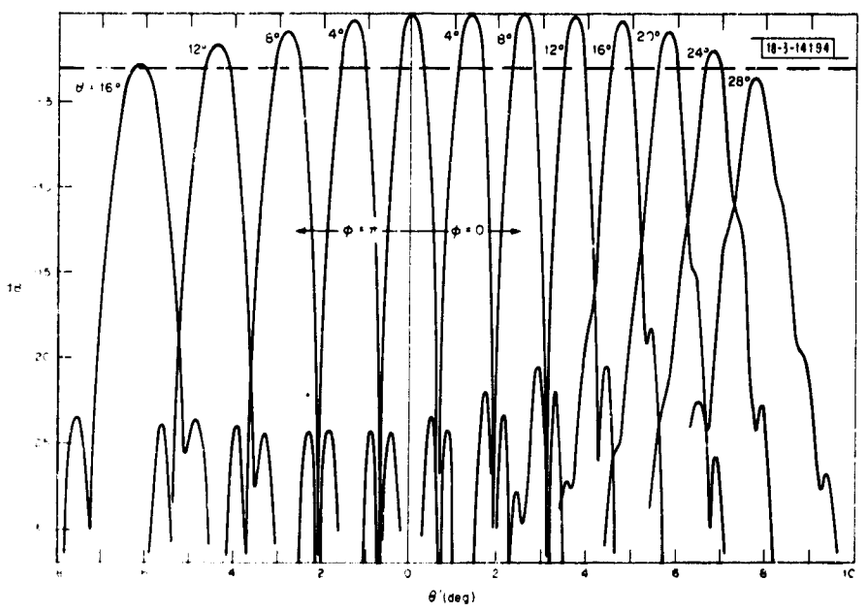

Fig. 7. Computed vertical-plane patterns for parameters of Fig. 5 with K = 1, C = 0.

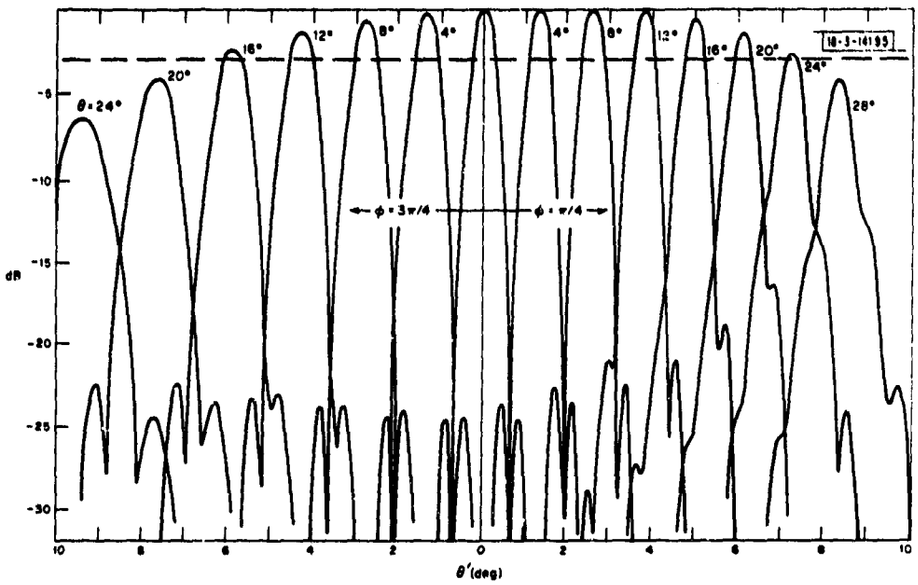

Fig. 8. Computed diagonal-plane patterns for parameters of Fig. 5 with K = 1, C = 0.

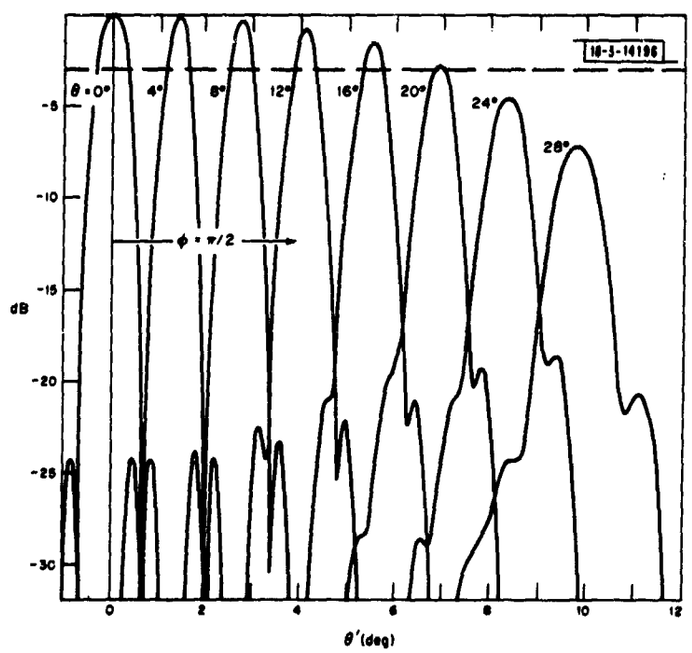

Fig. 9. Computed horizontal-plane patterns for parameters of Fig. 5 with K = 1, C = 0.

is that scan range is limited by phase aberrations. For $\varphi = \pi$, the beam broadens with very little distortion as scan is increased, indicating that spillover and aperture reduction are the principal causes of scan loss. Diagonal-plane patterns (Fig. 8) are very similar to the vertical patterns. The patterns in the horizontal plane – the only plane of symmetry – apparently have a measure of both spillover and phase aberrations. Note that in this plane, the patterns are well-defined and usable beyond the – 3-dB scan-loss point. Computed patterns with different distributions show similar characteristics. A more severe taper, for example $(1 - \rho^2)^2$, yields increased scan range and the "shoulders" on the scanned beam are less prominent. The uniform distribution results in less scan range and more pronounced distortion. Sidelobes at the – 3-dB scan-loss point for $\varphi = 0$ are 12 dB, and increase with greater scan.

Figure 10 illustrates the phase, spillover, and aperture reduction characteristics for a central strip in the vertical plane. The edge rays from the feed aperture are shown for +30°, 0° and – 16°. The aperture reduction and spillover for the – 16° case are consistent with the broad, distortion-free patterns of Fig. 7. Similarly, the large phase errors and relatively slight amount of spillover associated with the +30° case explain the pattern behavior in the $\varphi' = \pi$ plane.

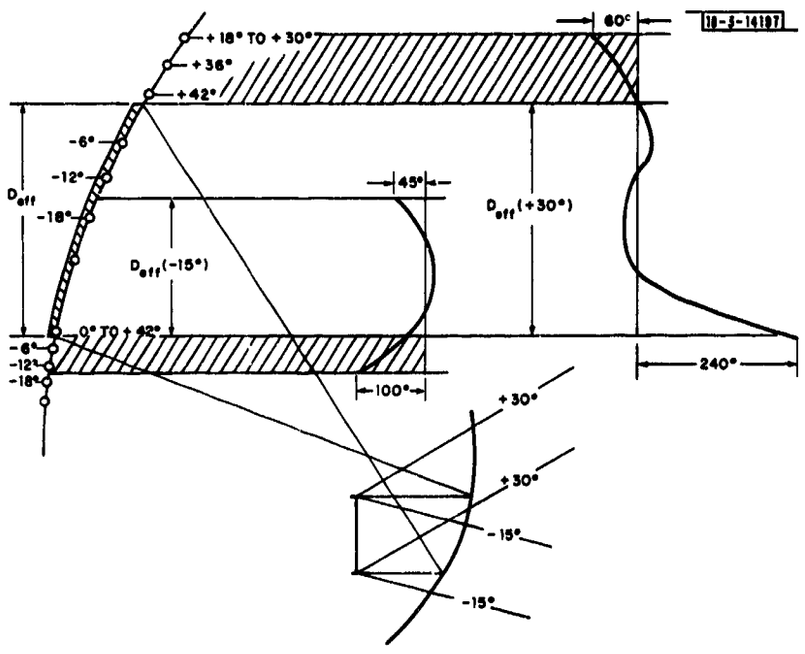

Fig. 10. Illustration of phase, spillover, and aperture reduction characteristics for central strip in vertical plane. D_{eff} for each case is as defined by extreme rays from feed aperture.

A substantial number of configurations were investigated by varying the parameters listed in Table I. In all cases, the general pattern characteristics – sidelobes, distortion, beam broadening, etc. – were similar to those found with the example of Fig. 5.

The following sections discuss the general characteristics of the system, and the significance of changing parameters on the scan range that can be achieved.

A. Reflector Sizes

The inequalities (6) and (7) define the outline of the reflectors. Removing these constraints is equivalent to using extended paraboloids for both reflectors. The scan range under these conditions is approximately the same for $\varphi = 0$ and $\varphi = \pi/2$, and increases for $\varphi = \pi$. However, the scan range in the latter case is principally limited by array blockage. We conclude that there is little, if any, increase in scan range realized by building an oversize main reflector.

Obviously, there is no point in having a subreflector larger than that required to avoid forward spillover. Calculations with and without the constraint (7) indicate that an elliptical subreflector, with its major axis in the horizontal plane, will yield the maximum scan range for a given subreflector area. The improvement is limited to the horizontal plane and is not of great significance. For the parameters of Fig. 5, an elliptical subreflector improves the scan range in the horizontal plane by approximately one beamwidth. Typically, the improvement is less than 10 percent.

For a fixed magnification, the scan range can be increased by increasing f_1 and f_2 in the same ratio. The subreflector diameter must increase accordingly to maintain the same forward spillover. Increasing the focal lengths by 25 percent in the example of Fig. 5 increases the cone of coverage from 7° to approximately 8.2°. The disadvantage of increasing scan range in this way is that the subreflector size must increase and the mechanical configuration becomes awkward.

B. Magnification

If the focal length f_1 is changed with all other parameters held fixed, the magnification and hence the effective aperture change in direct proportion. We found that, to a good approximation, the scan range in all planes is inversely proportional to the magnification, that is, the number of beamwidths scanned is constant. Also, to scan the secondary beam to the −3-dB scan-loss point, for example, requires approximately the same angle of tilt for the array.

Increasing the magnification with the effective aperture held constant (decreased array diameter) reduces the scan range in a more complex fashion. The reduction in the $\varphi = \pi$ plane is greatest. However, by adjusting the parameters which define the location of the array and subdish, the decrease is not nearly as great as the ratio of the magnifications. Figure 11 shows the scan range achieved with a magnification of 3.5 and the main aperture the same size as the example of Fig. 5. Note that the scan range is not greatly diminished from that shown in Fig. 6.

C. Frequency Dependence

Again using the parameters of Fig. 5, the frequency was halved and doubled to generate 1° and 1/4° beams. The resulting scan-coverage diagram is shown in Fig. 12. The scan range is least sensitive to frequency in the $\varphi = \pi$ plane where spillover and aperture reduction predominate. In general, the absolute scan range diminishes with increasing frequency but the number of beamwidths scanned increases. The coverage area shown in Fig. 12, for example, when measured in square beamwidths, is approximately 600 for the 1/2° beam and 1400 for the 1/4° beam, as defined by the −3-dB scan-loss criterion.

D. Array Position

The position of the array is not critical, although the favored position is as far back (ℓ large) and as high up (h small) as is consistent with avoiding (1) the blockage condition, and (2) excessive

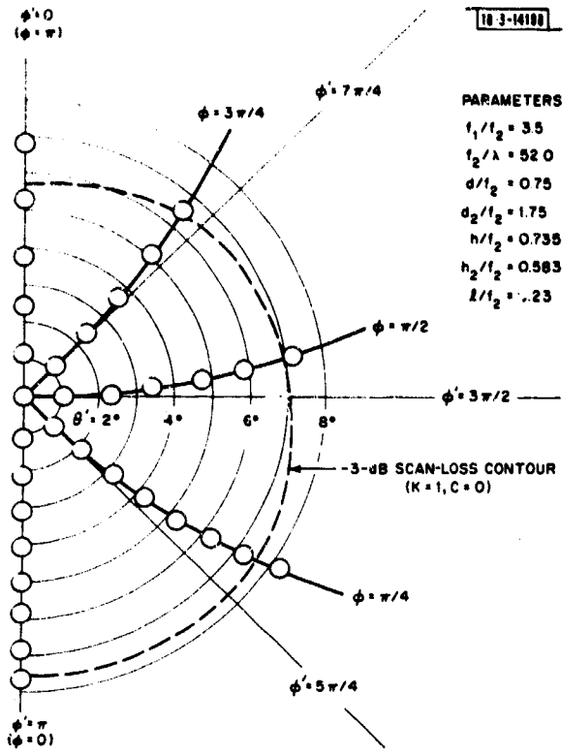

Fig. 11. Theoretical scan-coverage diagram with magnification of 3.5 and 1/2° beam.

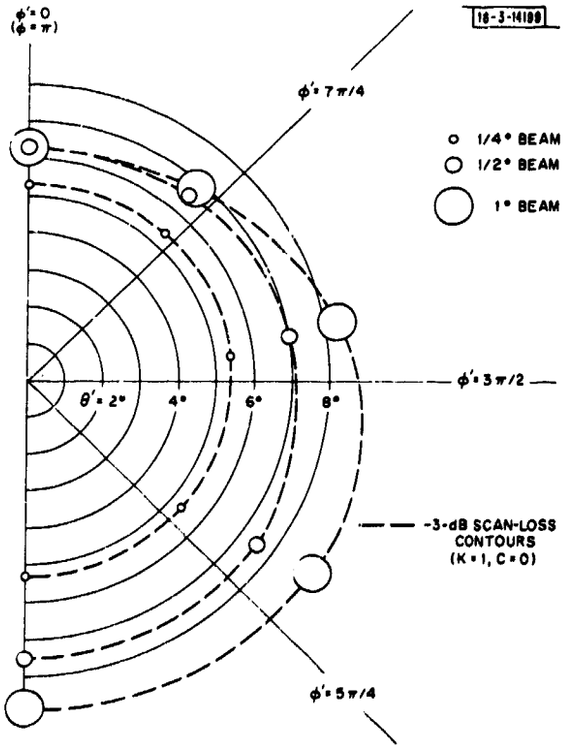

Fig. 12. Scan-coverage contours with parameters listed in Fig. 5. Parameter f_2/λ is adjusted for 1/4° and 1.0° beams.

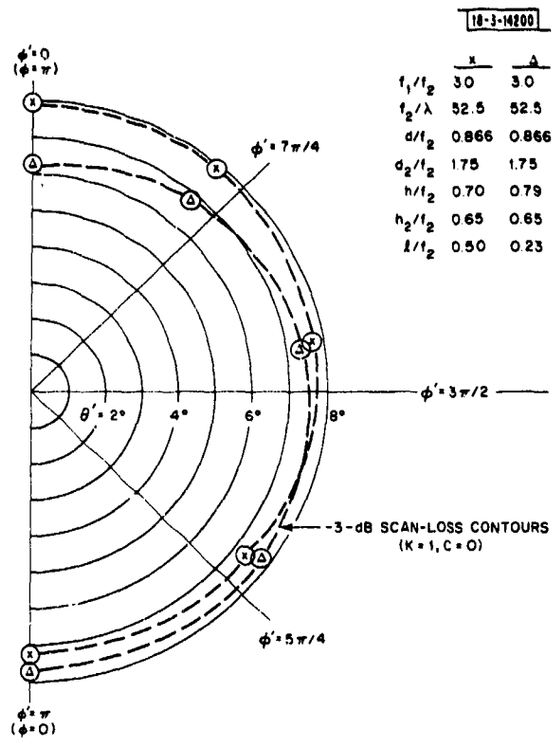

Fig. 13. Scan-coverage contours illustrating effect of array positioning.

forward spillover. Figure 13 shows the typical change in the scan contour as the array is repositioned. The parameters are similar to those of Fig. 5, with the subreflector diameter increased to 90λ. Most of the apparent increase in scan range for the "favored" position cannot be realized because of the blockage condition.

E. Difference Patterns

Figures 14 and 15 show difference patterns in the principal planes with full-wave sine distributions. System parameters are the same as those of Fig. 5. The variation in null depth and unbalance in the plane $\varphi = 0$ is the result of the asymmetrical phase and spillover characteristics in that plane.

The null fill-in with scan in the $\varphi = \pi$ plane is the result of spillover past the bottom of the main aperture, and aperture reduction (Fig. 10). The good balance is indicative of the absence of phase errors when scanning in this direction. Error patterns in the horizontal plane (Fig. 15) are not as well balanced but have deeper nulls and are relatively well behaved, just as with the corresponding sum patterns.

The null positions (Θ') and the locations of the difference pattern peaks (φ') coincide with the corresponding sum-pattern peaks to within approximately one-tenth of a beamwidth. This is the accuracy to which the computer program determines beam location.

IV. EXPERIMENT

Figure 16 shows the equipment used for an experimental demonstration. The reflectors are precision (surface tolerance ±0.010-inch peak) fiberglass laminates. The diameter of the main

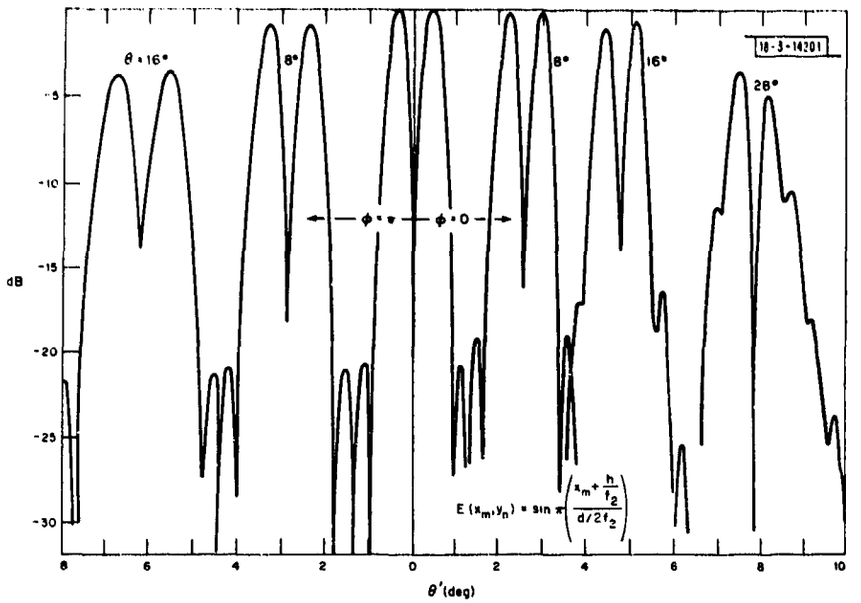

Fig. 14. Difference-pattern characteristics in vertical plane for example shown in Fig. 5.

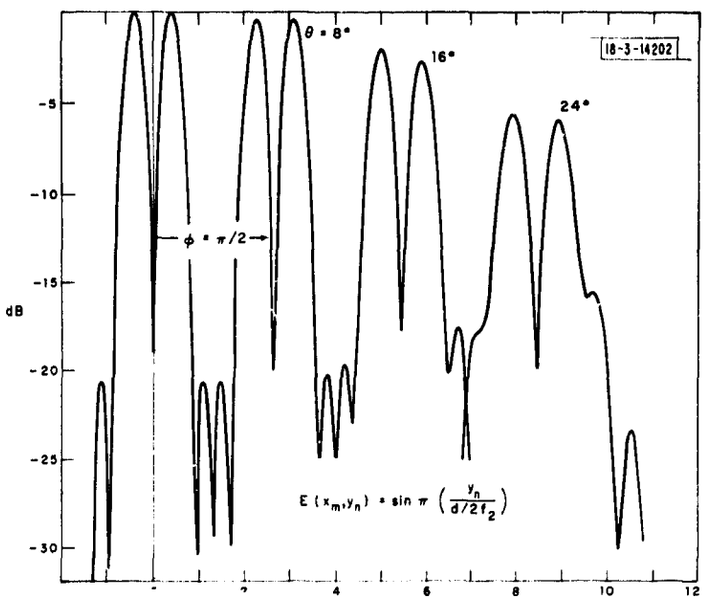

Fig. 15. Difference-pattern characteristics in horizontal plane for example shown in Fig. 5.

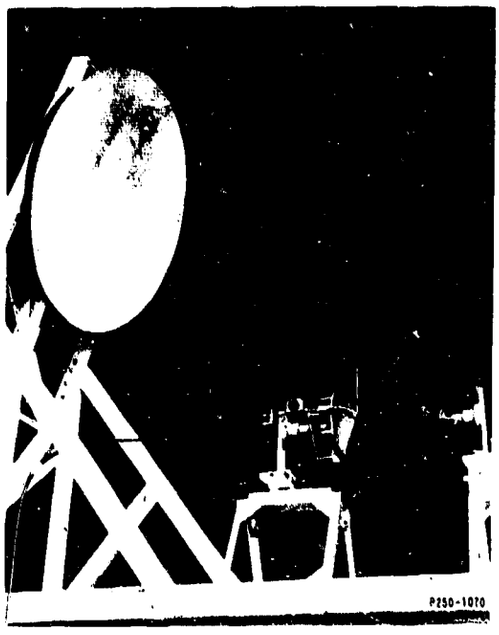

Fig. 16. Photograph of experimental equipment.

reflector is 48 inches (projected on the aperture plane) which generates a nominal 1/2° beam at the test frequency of 35.0 GHz. The array is simulated with a 12-inch-diameter paraboloid with a conventional focal point feed. The feed dish is mounted to permit rotation about any axis in its aperture plane. The subreflector is mounted in the same manner to facilitate initial focusing of the system. The following parameters were used in the experiment:

$$f_1/f_2 = 4.0$$

$$h_2/f_2 = 0.583$$

$$h/f_2 = 0.75$$

$$\ell/f_2 = 0.23$$

$$d_2/f_2 = 2.041$$

$$d/f_2 = 0.875$$

$$f_2/\lambda = 40.71$$

Figure 17 shows the measured boresight patterns. The primary patterns have similar characteristics, i.e., sidelobes are >24.0 dB and the H-plane pattern is approximately 10 percent broader than the E-plane pattern. This indicates that the feed-aperture distribution is accurately reproduced in form over the main aperture. The computed and measured positions of the secondary beams are shown in Fig. 18. Agreement is to within approximately one-tenth of a beamwidth, which is about the limit of experimental accuracy. Comparisons of experimental and theoretical patterns (computed using the parameters listed above with K = 1, C = 0) in the vertical and horizontal planes are shown in Figs. 19 through 22. When the feed dish is scanned downward in the vertical plane ($\varphi = \pi$), the top of the feed aperture is moved into the region of high-field density,

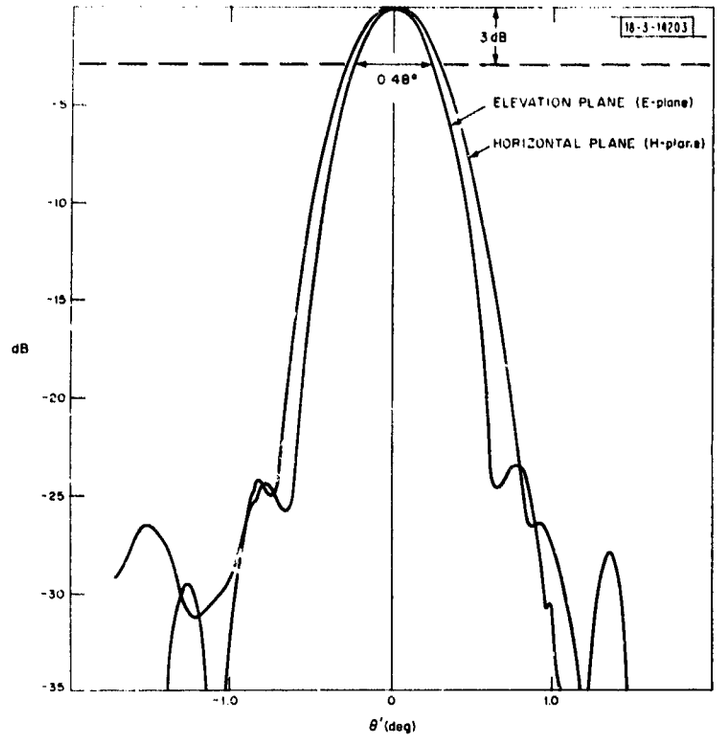

Fig. 17. Measured boresight patterns in two principal planes at 35.0 GHz.

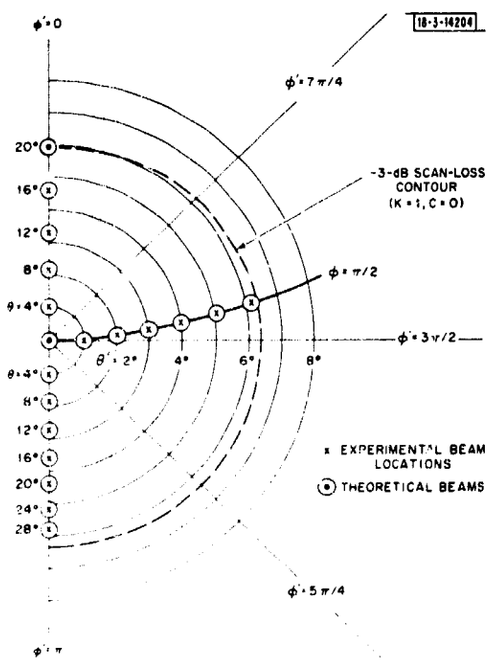

Fig. 18. Comparison of theoretical and experimental secondary-beam positions.

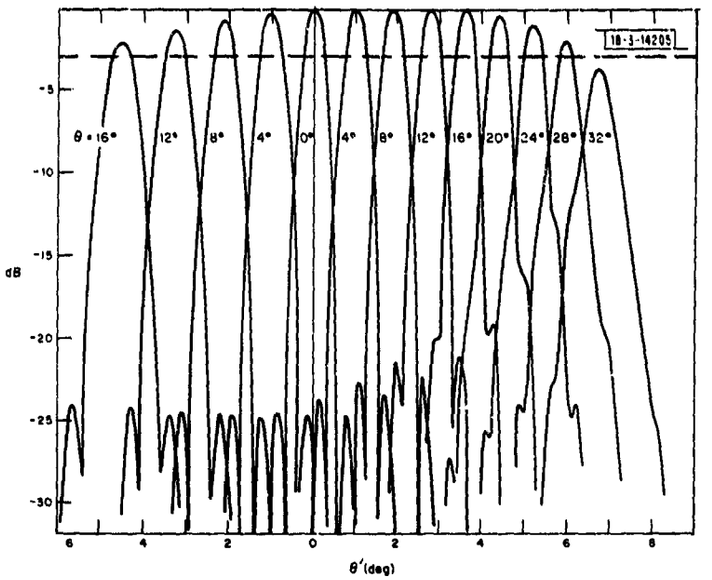

Fig. 19. Theoretical vertical-plane patterns with K = 1, C = 0. Parameters are those used in experiment (see p. 15).

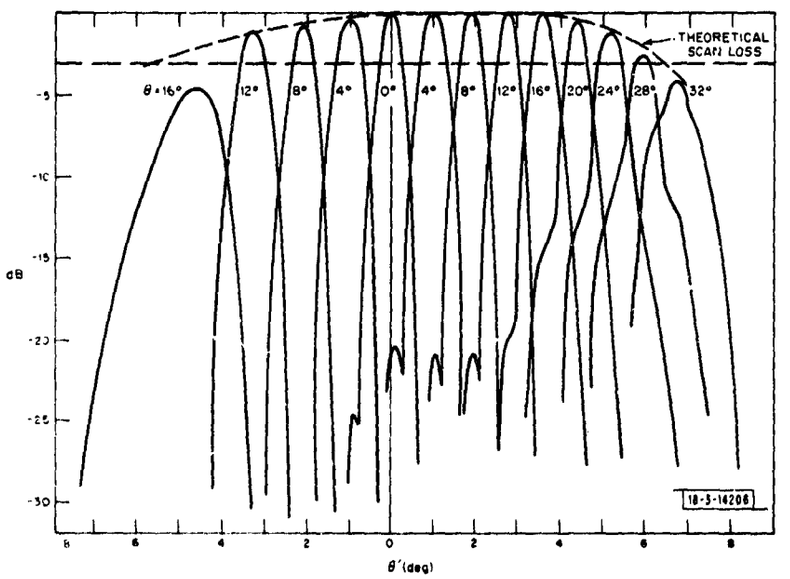

Fig. 20. Measured vertical-plane patterns.

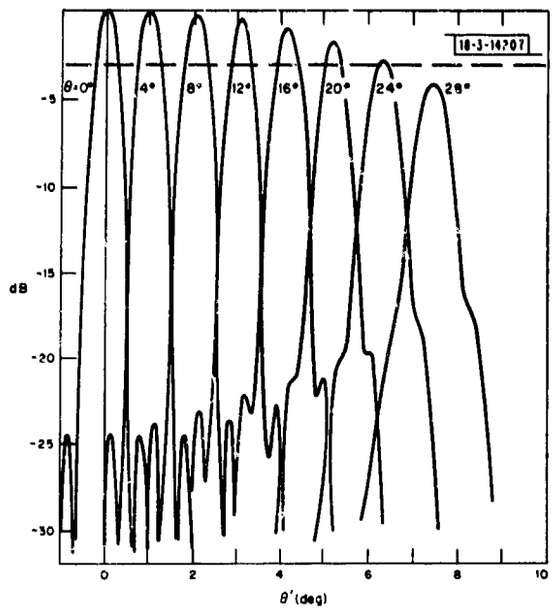

Fig. 21. Theoretical horizontal-plane patterns with K = 1, C = 0. Parameters are those used in experiment (see p. 15).

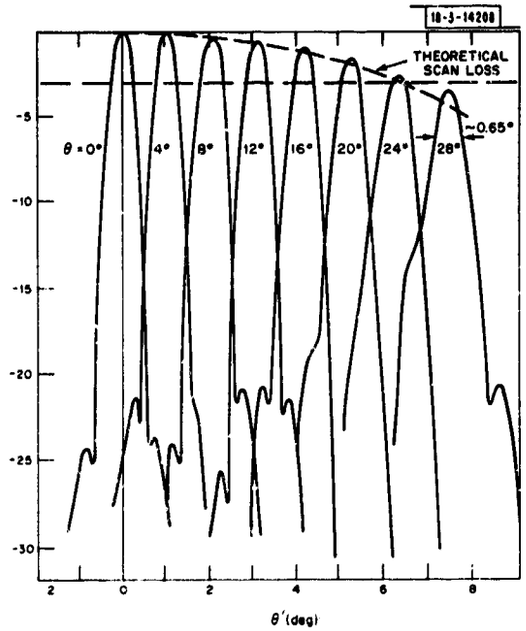

Fig. 22. Measured horizontal-plane patterns.

hence, the blockage condition occurs sooner than would be the case with an electronically scanned array.

In general, the theoretical and the measured characteristics are in close agreement. Scan range, beam broadening and sidelobe behavior are essentially as predicted. Lack of agreement as the result of different tapers (K = 1, C = 0 was used for the computations and the actual distribution is not circularly symmetric) and the simulation of phase scanning with mechanical scan is negligible. A $\cos\theta$ factor in projected aperture is the principal difference between mechanical and electronic scan which should not be of great significance in view of the spillover-phase characteristics depicted in Fig. 10.

Patterns were measured in the plane orthogonal to the plane of scan at the extreme scan positions. In all cases, sidelobes were lower and beamwidths were equal to or less than the corresponding pattern in the plane of scan.

V. SUMMARY AND DISCUSSION

The combination of array and reflector techniques in the near-field Gregorian configuration has been demonstrated to perform exceptionally well as a limited-field-of-view system. The important characteristics of the system are summarized as follows:

Although the feed array is scanned with simple row-column beam-steering commands, the nonlinear relationship between the θ, φ and θ', φ' coordinates introduces some complication to the beam-steering unit. Polynomial curve-fitting techniques or a "look-up" table will be required to locate the position of the main beam.

The main aperture is completely utilized for the boresight beam. There appears to be little, if any, increase in scan range with an oversized main reflector.

The sidelobes are well behaved in all planes of scan. The effects of "coma" are noticeably absent.

Varying the magnification (changing f_1) with all other parameters held fixed changes the effective aperture in direct proportion. The scan range measured in beamwidths is constant under these conditions.

With an effective aperture and magnification held fixed, the scan range can be improved by increasing the focal lengths in the same proportion. This results in a larger subreflector and a more awkward mechanical configuration.

The frequency dependence of scan range follows a complex fractional power law which is dependent on the choice of parameters and the plane of scan. In general, the absolute scan range diminishes but the number of beamwidths scanned increases with increasing frequency.

The related near-field Cassegrainian system[1] is better suited for modifying a radar in the field for limited-scan capability. The offset-feed geometry is less suitable for this purpose and presents a less attractive geometry for pedestal mounting. However, performance characteristics – scan range, sidelobes, efficiency, etc. – are considerably improved.

Further improvement in performance may be achieved by shaping the subreflector, i.e., using a computed nonparabolic contour, to minimize phase aberrations. This is suggested by the fact that the extremes of scan use different portions of the oversized subreflector. This approach has not been investigated.

The analysis considers a coaxial reflector system. The feed and subreflector could be rotated as a unit about the focal point without affecting collimation for the boresight beam. A slight amount of space attenuation would be introduced. The possibility of improving scan characteristics with such a rotation is also open for study.

ACKNOWLEDGMENT

The author wishes to thank Mr. Carl Blake and Dr. G.N. Tsandoulas for encouragement and helpful discussions, Miss Janet M. Reid for writing the computer program, and Mr. E.F. Pelrine and Mr. L.J. Gerrior for assistance with the measurements effort.

REFERENCES

1. W.D. Fitzgerald, "Limited Electronic Scanning with a Near-Field Cassegrainian System," Technical Report 484, Lincoln Laboratory, M.I.T. (24 September 1971).
2. E.A. Dudkovsky, "A System for Exciting Large Parabolic Antennas," Russian Patent No. 146365 (1962).
3. G.E. Skahill, L.K. DeSize and P.J. Wilson, "Electronically Steerable Field Reflector Antenna Techniques," Technical Report RADC-TR-66-354 (August 1966).
4. C.C. Allen, "Numerical Integration Methods for Antenna Pattern Calculations," Trans. IRE, PGAP AP-7 Suppl., S387-S401 (1959).

APPENDIX
RAY-TRACING PROCEDURE

Referring to Fig. 3, we compute the path length of a general ray from a point $(x, y, -\ell)$ on the array aperture through the two-reflector system to the corresponding point in the main aperture plane $(x', y', z' = 0)$. The origin of the coordinate system coincides with the focal point of both reflectors. The main aperture plane is arbitrarily chosen to be in the focal plane or the x-y plane. A point on the subreflector is denoted (x_2, y_2, z_2). Similarly, (x_1, y_1, z_1) defines a point on the main reflector. The equation of the main reflector is

$$z_1 = \frac{x_1^2 + y_1^2}{4f_1} - f_1 \tag{A-1}$$

and the equation of the subreflector is

$$z_2 = f_2 - \frac{x_2^2 + y_2^2}{4f_2} \quad . \tag{A-2}$$

The spherical coordinates θ, φ define the direction of the general ray emerging from the aperture. This ray is perpendicular to the assumed linear phase tilt and hence is parallel to

$$\bar{a}\bar{b} = \bar{i} \sin\theta \cos\varphi + \bar{j} \sin\theta \sin\varphi + \bar{k} \cos\theta \quad . \tag{A-3}$$

Lower-case letters denote unit vectors, and i, j, k are the unit vectors parallel to the coordinate axes.

The component ray from the point A on the array to the point B on the subreflector is given by

$$\overline{AB} = \bar{i}(x_2 - x) + \bar{j}(y_2 - y) + \bar{k}(z_2 + \ell) \quad . \tag{A-4}$$

The unit vector $\overline{AB}/|AB|$ is equated with Eq. (A-3). This yields three equations which define a line in three-dimensional space. Only two of these equations are independent:

$$\tan\varphi \, (x_2 - x) = (y_2 - y)$$

$$\frac{1}{\tan\theta \cos\varphi} \, (x_2 - x) = (z_2 + \ell) \quad . \tag{A-5}$$

Solving Eqs. (A-5) and (A-2) gives the coordinates of the first point of reflection B:

$$x_2 = \frac{-B \pm \sqrt{B^2 - 4AC}}{2A}$$

$$y_2 = y + (x_2 - x) \tan\varphi$$

$$z_2 = f_2 - \frac{x_2^2 + y_2^2}{4f_2} \tag{A-6}$$

where

$$A = (1 + \tan^2 \varphi)$$

$$B = \left(2y \tan \varphi - 2x \tan^2 \varphi + \frac{4f_2}{\tan\theta \cos \varphi}\right)$$

$$C = \left[y^2 + x^2 \tan^2 \varphi - \frac{4f_2 x}{\tan\theta \cos \varphi} - 4f_2(f_2 + \ell) - 2xy \tan \varphi\right] \quad .$$

Snell's law of reflection relates the incident, reflected, and normal unit vectors at the point x_2, y_2, z_2 on the subreflector

$$\overline{bc} = \overline{ab} - 2\bar{n}_2(\bar{n}_2 \cdot \overline{ab}) \quad . \tag{A-7}$$

The unit normal ($\bar{n}_2$) on the subreflector surface is

$$\bar{n}_2 = -\left(\frac{\bar{i}x_2 + \bar{j}y_2 + \bar{k}(2f_2)}{\sqrt{x_2^2 + y_2^2 + 4f_2^2}}\right) \quad . \tag{A-8}$$

By using Eq. (A-3), the components of the unit vector $\overline{bc}$ are

$$(bc)_x = \sin\theta \cos \varphi - \frac{2x_2}{x_2^2 + y_2^2 + 4f_2^2} [x_2 \sin\theta \cos \varphi + y_2 \sin\theta \sin \varphi + 2f_2 \cos\theta]$$

$$(bc)_y = \sin\theta \sin \varphi - \frac{2y_2}{x_2^2 + y_2^2 + 4f_2^2} [x_2 \sin\theta \cos \varphi + y_2 \sin\theta \sin \varphi + 2f_2 \cos\theta]$$

$$(bc)_z = \cos\theta - \frac{4f_2}{x_2^2 + y_2^2 + 4f_2^2} [x_2 \sin\theta \cos \varphi + y_2 \sin\theta \sin \varphi + 2f_2 \cos\theta] \quad . \tag{A-9}$$

The component ray $\overline{BC}$ is

$$\overline{BC} = \bar{i}(x_1 - x_2) + \bar{j}(y_1 - y_2) + \bar{k}(z_1 - z_2) \quad . \tag{A-10}$$

Equating the unit vectors $\overline{BC}/|BC| = \overline{bc}$, we again have three equations defining a line in space, only two of which are independent. Thus,

$$\frac{(bc)_y}{(bc)_x}(x_1 - x_2) = y_1 - y_2$$

$$\frac{(bc)_z}{(bc)_x}(x_1 - x_2) = z_1 - z_2 \quad .$$

Solving Eqs. (A-11) and (A-1) gives the coordinates of the point [illegible] tor C:

$$x_1 = \frac{-B' \pm \sqrt{B'^2 - 4A'C'}}{2A'}$$

$$y_1 = y_2 + \frac{(bc)_y}{(bc)_x}(x_1 - x_2)$$

$$z_1 = \frac{x_1^2 + y_1^2}{4f_1} - f_1 \qquad \text{(A-12)}$$

where

$$A' = \left\{1 + \left[\frac{(bc)_y}{(bc)_x}\right]^2\right\}$$

$$B' = \left\{2y_2 \frac{(bc)_y}{(bc)_x} - 2x_2 \left[\frac{(bc)_y}{(bc)_x}\right]^2 - 4f_1 \frac{(bc)_z}{(bc)_x}\right\}$$

$$C' = \left\{4f_1 x_2 \frac{(bc)_z}{(bc)_x} - 2x_2 y_2 \frac{(bc)_y}{(bc)_x} + x_2^2 \left[\frac{(bc)_y}{(bc)_x}\right]^2 + y_2^2 - 4f_1(f_1 + z_2)\right\} .$$

Snell's law of reflection at the point x_1, y_1, z_1 is written

$$\overline{cd} = \overline{bc} - 2\bar{n}_1(\bar{n}_1 \cdot \overline{bc}) \quad . \qquad \text{(A-13)}$$

The unit normal at the point of reflection on the main reflector is

$$\bar{n}_1 = \frac{\bar{i}(-x_1) + \bar{j}(-y_1) + \bar{k}(2f_1)}{\sqrt{x_1^2 + y_1^2 + 4f_1^2}} \quad . \qquad \text{(A-14)}$$

By using Eqs. (A-9) and (A-14), the components of the unit vector $\overline{cd}$ are found:

$$(cd)_x = (bc)_x - \frac{2x_1}{x_1^2 + y_1^2 + 4f_1^2}[x_1(bc)_x + y_1(bc)_y - 2f_1(bc)_z]$$

$$(cd)_y = (bc)_y - \frac{2y_1}{x_1^2 + y_1^2 + 4f_1^2}[x_1(bc)_x + y_1(bc)_y - 2f_1(bc)_z]$$

$$(cd)_z = (bc)_z + \frac{4f_1}{x_1^2 + y_1^2 + 4f_1^2}[x_1(bc)_x + y_1(bc)_y - 2f_1(bc)_z] \quad . \qquad \text{(A-15)}$$

The component ray $\overline{CD}$ is

$$\overline{CD} = \bar{i}(x' - x_1) + \bar{j}(y' - y_1) + \bar{k}(-z_1) \qquad \text{(A-16)}$$

where the main aperture plane is defined as the plane $z' = 0$. The equation $\overline{CD}/|CD| = \overline{cd}$ yields two equations which are sufficient to determine the coordinates in the aperture plane $z' = 0$:

$$\frac{(cd)_y}{(cd)_x}(x' - x_1) = y' - y_1$$

$$\frac{(cd)_z}{(cd)_x}(x' - x_1) = -z_1$$

from which

$$x' = x_1 - \frac{(cd)_x}{(cd)_z} z_1$$

$$y' = y_1 + \frac{(cd)_y}{(cd)_x}(x' - x_1)$$

$$z' = 0 \quad .$$

The optical path length is simply the sum of the component path lengths. Hence,

$$L = |\overline{AB}| + |\overline{BC}| + |\overline{CD}| \qquad \text{(A-17)}$$